Physics in Medicine & Biology

PAPER

Pairwise hemorrhage-brain region interaction-driven hemorrhagic stroke assessment in CT

To cite this article: Wei Liang *et al* 2025 *Phys. Med. Biol.* **70** 015006

IOP Publishing Phys. Med. Biol. 70 (2025) 015006 https://doi.org/10.1088/1361-6560/ad9ce3

Physics in Medicine & Biology

IPEM Institute of Physics and Engineering in Medicine

PAPER

RECEIVED
14 August 2024

REVISED
17 November 2024

ACCEPTED FOR PUBLICATION
10 December 2024

PUBLISHED
24 December 2024

Pairwise hemorrhage-brain region interaction-driven hemorrhagic stroke assessment in CT

Wei Liang[1,4], **Haixiong Wu**[2,4], **Hongbin Guo**[1], **Zhanyao Huang**[1], **Shibin Liang**[1], **Jinhuang Zhang**[1], **Huiling Zhang**[1], **Xiangyuan Ma**[1,*] **and Zibi Xu**[3,*]

[1] Department of Biomedical Engineering, College of Engineering, Shantou University, Shantou, People's Republic of China
[2] Longdu Central Hospital, Chenghai District, Shantou, People's Republic of China
[3] The Second Affiliated Hospital of Shantou University Medical College, Shantou, People's Republic of China
[4] Authors contributed equally to this work.
[*] Authors to whom any correspondence should be addressed.

E-mail: maxiangyuan@stu.edu.cn and 542537341@qq.com

Keywords: computer-aided diagnosis, deep learning, hemorrhagic stroke

Abstract

Objective. Hemorrhagic stroke is a major global health problem requiring rapid and accurate diagnosis for effective treatment. Despite advances, current computer-aided diagnosis (CAD) frameworks rarely account for the functional impacts of hemorrhages on specific critical brain regions and lack the detailed assessments essential for precise treatment. To provide detailed insights into hemorrhages, we aim to propose a CAD framework for in-depth hemorrhagic stroke assessment in computed tomography (CT). The framework includes segmenting hemorrhages and critical brain regions, intraparenchymal hemorrhage (IPH) classification for identifying hemorrhages in critical brain regions and detecting hemorrhage volume. *Approach.* To capture the complex interactions between hemorrhages and critical brain regions, we developed the pairwise hemorrhage-brain regions interaction (PHRI) Network. Its emphasis a novel interaction head that integrates feature on hemorrhages, brain regions, and their interdependencies, enabling the model to learn these relationships during training. In addition, a Global-Local Fusion Unit was introduced to provide with image-wide contextual information, and an uncertainty-weighted loss method was utilized to simultaneously optimise the multitask framework. With institutional review board approval, an in-house hemorrhagic stroke dataset was collected, including 2,764 CT slices from 99 patients. A five-fold cross-validation was used to train and test the models. *Main Results.* The proposed PHRI network was experimentally validated to effectively extract hemorrhage brain region interactions, thereby significantly outperforming several state-of-the-art models in both hemorrhage and critical brain region segmentation, with an average Dice of 0.9064 $\pm$ 0.1079 ($P < 0.05$), as well as in IPH classification, with an F1-Score of 0.8366. Additionally, the framework demonstrated good performance in hemorrhage volume detection, with an intraclass correlation coefficient of 0.981. *Significance.* This study introduces a CAD framework for hemorrhagic stroke assessment, offering a novel approach that emphasizes relationships between hemorrhages and critical brain regions.

1. Introduction

Stroke is the second leading cause of death globally after heart disease, and has a profound impact on global health (World Stroke Organization 2022). Beyond mortality, stroke is a primary contributor to disability, imposing long-term rehabilitation challenges on survivors and diminishing their quality of life (Feigin 2021). There are two main types of stroke: ischemic and hemorrhagic. Hemorrhagic strokes are typically more severe, exhibiting a higher mortality rate and a higher severe disability rate (Kaae Andersen *et al* 2009). Specifically, hemorrhagic stroke is initiated by cerebral blood vessel rupture, resulting in elevated brain tissue pressure, unconsciousness, and hemiplegia (Qureshi *et al* 2001).

To address the high mortality rate of stroke, timely and effective diagnosis is critical for initiating immediate treatment and preventing further damage (George 2017). Especially for hemorrhagic strokes, prompt diagnosis, and treatment are crucial to prevent rapid hematoma expansion in the brain and the associated risk of severe outcomes (McGurgan *et al* 2021). Medical imaging tools, such as computed tomography (CT) or magnetic resonance imaging (MRI), are commonly used to confirm the diagnosis of strokes and determine the location and extent of bleeding. Compared to MRI, CT is the preferred initial imaging choice in the acute emergency scenario of hemorrhagic stroke because of its swiftness and cost-effectiveness (Macellari *et al* 2014, Hakimi and Garg 2016, Al Fauzi 2020). Notably, the pursuit of aiding clinicians in achieving quicker stroke diagnoses using CT scans without sacrificing accuracy remains a significant topic.

Recently, computer-aided diagnosis (CAD) systems have emerged as effective tools to aid clinicians in swift and accurate diagnoses (Fujita 2020, Manjurul Ahsan *et al* 2022, Zhang *et al* 2024). Current CAD systems designed for hemorrhagic strokes focus mainly on segmenting hemorrhagic lesions and classifying intracranial hemorrhage (ICH) subtypes. Classification of ICH subtypes is fundamental for guiding the treatment of hemorrhagic strokes. Various deep learning models have been developed to accurately classify ICH subtypes, including intraparenchymal (IPH), intraventricular, epidural, subdural, and subarachnoid hemorrhage (Chilamkurthy *et al* 2018, McLouth *et al* 2021, Wang *et al* 2022, Arman *et al* 2023, ElZemity *et al* 2023, Umapathy *et al* 2023). For instance, Chilamkurthy *et al* (2018), Arman *et al* (2023), and Umapathy *et al* (2023) employed CNN architecture for ICH classification. In addition, ElZemity *et al* (2023) and Wang *et al* (2022) employed Transformer-based architecture for hemorrhage detection and classification.

Although the aforementioned deep learning models have demonstrated promising accuracy, they seldom consider the functional impacts of hemorrhages on specific critical brain regions, thereby constraining the personalization and precision of treatments. Specifically, hemorrhage in various IPH regions can cause diverse clinical symptoms and complications. For example, hemorrhage in the basal ganglia can result in cognitive decline (Su *et al* 2007). Thalamus hemorrhage is also known to predominantly affect cognition (Temel *et al* 2021). Movement disorders have also been found in patients with strokes in the thalamus and basal ganglia (Park 2016). In addition, brainstem hemorrhages can result in significant disruptions in consciousness, central hyperthermia, and a high risk of neurological complications (Chen 2021). In the case of the cerebellum, hemorrhage may impair balance and coordination (Ibrahim *et al* 2022).

Therefore, to offer a more nuanced assessment of hemorrhagic strokes, a finer classification of IPH is essential in clinical practice. The IPH classification identifies hemorrhages in critical brain regions, including the basal ganglia, thalamus, brainstem, and cerebellum (Hillal *et al* 2022), which are known for their unique location and important functions (Su *et al* 2007, Park 2016, Chen 2021, Temel *et al* 2021, Ibrahim *et al* 2022). Such specificity is paramount for customizing therapeutic interventions, acknowledging that the exact hemorrhage location and its relationship with critical brain regions significantly influence treatment strategies. (Broderick 2007, Hostettler *et al* 2019, Zhu Suiqiang and Liying 2019, Al Fauzi 2020, Chen 2021, Lv and Wei 2021).

To effectively and accurately classify IPH, it is necessary to design CAD methods capable of capturing the relationships between hemorrhages and critical brain regions. In clinical practice, the relationships between hemorrhage and brain regions can be categorized into non-contact, contact due to hemorrhage spread, and hemorrhage originating within a brain region. A hemorrhage may be in contact with multiple brain regions, but only a hemorrhage originating within a brain region is considered IPH. This originating relationship between the brain regions and the hemorrhage can be considered an interaction. For instance, as shown in figure 1, a hemorrhage may be in contact with more than one brain region, but this does not necessarily indicate interaction, i.e. it does not necessarily mean that the corresponding brain regions have a hemorrhage. Therefore, modeling an effective methodology for capturing hemorrhage-brain region relationships is crucial.

Capturing such relationships requires accurate segmentation of hemorrhage and critical brain regions, as well as robust modeling of their interaction. However, current hemorrhage-related segmentation methods primarily focus on independently segmenting hemorrhagic lesions or brain regions and lack a dedicated design to specifically model hemorrhage-brain interactions. For instance, Sugino *et al* (2024) implemented convolutional neural networks (CNNs) with various skip connection methods to segment the basal ganglia. Shu *et al* (2022) applied a U-Net architecture enhanced with efficient channel attention for the segmentation of the cerebellum. Similarly, Retuci Pinheiro *et al* (2023) employed U-Net for thalamus segmentation. On the hemorrhagic segmentation front, Dhar (2020), Peng *et al* (2022), Coorens *et al* (2023) relied on U-Net and its derivatives. Furthermore, Nijiati *et al* (2022), Xiao *et al* (2024), and Piao *et al* (2023) explored the use of Transformers for hemorrhage segmentation. Despite the proven effectiveness of these methodologies, there is a lack of networks that explicitly model the interplay between hemorrhages and specific brain regions. This limitation hinders the ability to enhance the performance of the hemorrhagic stroke assessment.

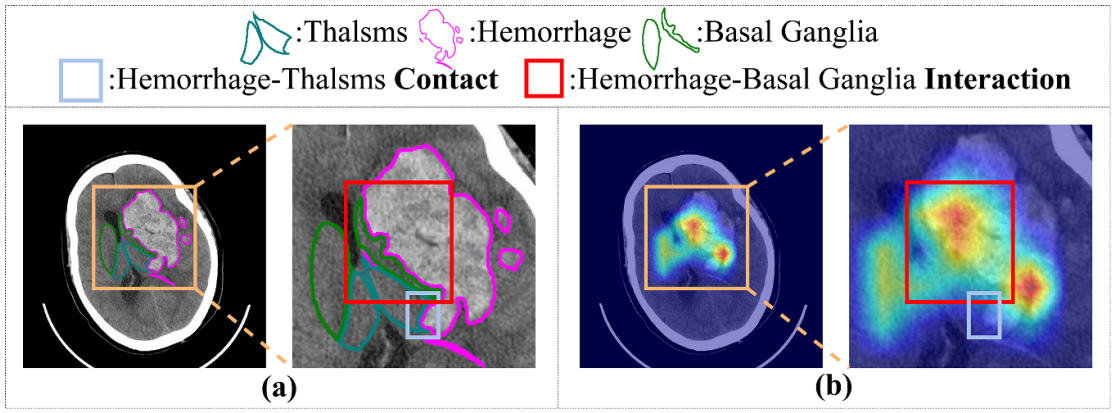

Figure 1. As depicted in sub-figure (a), in a scenario where a hemorrhage contacts both the basal ganglia and the thalamus, the gold standard classifies this IPH as a basal ganglia hemorrhage. To validate the interaction, we employed Gradient-weighted class activation mapping (Grad-CAM) (Selvaraju *et al* 2019) on our proposed network, as illustrated in sub-figure (b). The visualization highlights the hemorrhage and the bilateral basal ganglia, indicating that the hemorrhage is predominantly associated with the basal ganglia.

In this study, our objective is to investigate an effective methodology for capturing hemorrhage-brain region relationships, enabling accurate segmentation of hemorrhages and critical brain regions, as well as precise classification of IPH. Significant progress has been made in understanding complex interactions within the human-object interaction (HOI) detection task (Cho *et al* 2023, Park *et al* 2023, Tu *et al* 2023, Zhang *et al* 2023). For example, Kim *et al* (2022) and Tamura *et al* (2021) proposed frameworks featuring an interaction detection head to elucidate the relationships between humans and objects.

Motivated by the aforementioned HOI concepts, we present a pairwise hemorrhage-brain regions interaction (PHRI) network. The proposed network can capture the relationships between hemorrhages and critical brain regions. Importantly, we apply the proposed network to conduct an in-depth assessment of hemorrhagic strokes. The main contributions of this study are summarized as follows:

(i) To conduct an in-depth assessment of hemorrhagic strokes, we proposed a framework including hemorrhage segmentation, critical brain regions segmentation, IPH subtypes classification, and hemorrhage volume detection.
(ii) To efficiently capture and exploit the relationships between hemorrhage and critical brain regions, we developed a PHRI network. With the effect of sufficient hemorrhage-brain regions interaction, the performance of hemorrhagic stroke assessment can be improved. In computer vision, the HOI field plays a crucial role in exploring the interactions. Building on this, we introduced this concept to medical imaging for the first time.
(iii) To further validate the interaction capabilities of PHRI, we implemented a post-segmentation classification approach based on clinical experience. Experimental results demonstrate that our interaction-based method models the relationships between hemorrhages and various brain regions more effectively, leading to enhanced classification robustness.
(iv) To enhance the effectiveness of extracting image-wide contextual information, we introduced a flexible global-local fusion unit (GLFU). This unit is designed to integrate global and local information and can serve as a replacement for convolutional blocks.

The rest of the paper is structured as follows: section 2 describes the proposed framework, as well as the additional clinical experience-based classification method. Section 3 presents the experimental setup, compares the proposed method with state-of-the-art approaches, and presents several experiments. The paper concludes with a discussion and a brief conclusion in sections 4 and 5.

2. Method

This section introduces the hemorrhagic stroke assessment framework, illustrated in figure 2. The framework consists of two main phases: Phase 1, the PHRI network, and Phase 2, the Hemorrhage Assessment. In Phase 1, the PHRI network processes an input CT image and produces both a segmentation map and an interaction vector. The segmentation map delineates both hemorrhagic and brain regions, while the interaction vector captures the interactions between the hemorrhage and the corresponding brain regions. In Phase 2, these

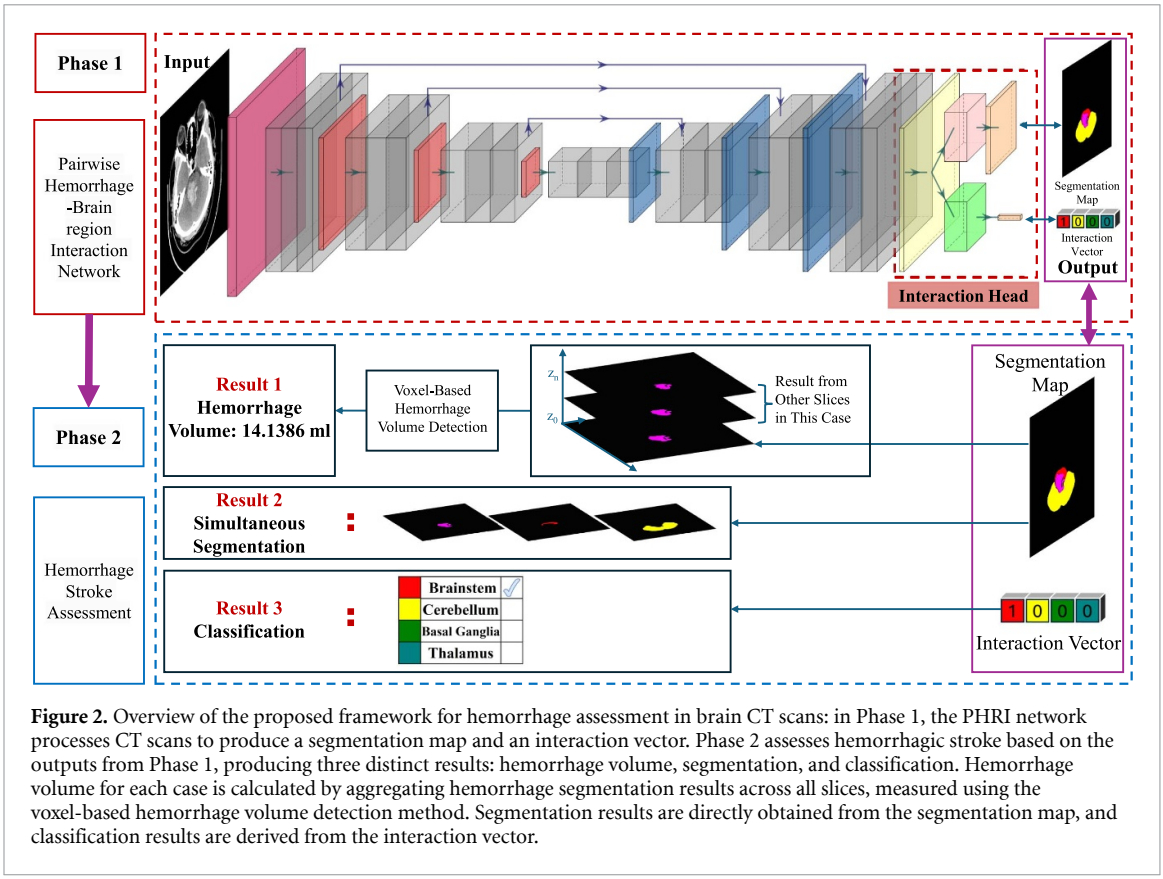

Figure 2. Overview of the proposed framework for hemorrhage assessment in brain CT scans: in Phase 1, the PHRI network processes CT scans to produce a segmentation map and an interaction vector. Phase 2 assesses hemorrhagic stroke based on the outputs from Phase 1, producing three distinct results: hemorrhage volume, segmentation, and classification. Hemorrhage volume for each case is calculated by aggregating hemorrhage segmentation results across all slices, measured using the voxel-based hemorrhage volume detection method. Segmentation results are directly obtained from the segmentation map, and classification results are derived from the interaction vector.

outputs are utilized for a comprehensive hemorrhage assessment, generating three distinct results: the total hemorrhage volume for each case, measured using the Voxel-Based Hemorrhage Volume Detection method, which leverages the hemorrhage segmentation from the segmentation map; segmentation results for hemorrhages and brain regions obtained directly from the segmentation map; and classification results derived from the interaction vector. Together, these outputs provide a detailed, region-specific assessment of hemorrhage for clinical evaluation. In addition to the PHRI network, we introduce a post-segmentation classification approach based on clinical experience to classify the IPH subtype from the post-segmentation result. This approach allows for comparison with the PHRI classification output. A more detailed explanation of the approach can be found in the Clinical Experience-Based Classification Method section.

2.1. PHRI network

As illustrated in figure 3, this study introduces the PHRI network, which advances upon the foundational U-Net architecture (Ronneberger *et al* 2015), preserving its encoder-decoder framework while innovating with the inclusion of a hemorrhage-brain regions interaction head. The innovative interaction head replaces the traditional expanding layer for precise hemorrhage-brain region relationships capturing. In addition, to train the hemorrhage-brain regions interaction (HRI) feature map inside the interaction head efficiently, we introduced a GLFU and a series of loss optimization methods. GLFU is a unit that integrates convolution and self-attention mechanisms to capture global and local information, respectively. To train pairwise interactions more efficiently in the training phase, we utilized the uncertainty weighting loss method (Kendall *et al* 2018) for simultaneous optimization. More detailed explanations of these network components are provided in the following sub-sections.

The architecture of the proposed PHRI network is based on an encoder-decoder structure. Initially, brain CT images are embedded and subsequently processed through three-layer successive encoder blocks during the encoding phase. Each scale encoder block processes the feature maps through three GLFUs, which are then followed by a down-sampling layer. The specifically designed embedding employs a combinationof convolutional layers, Gaussian Error Linear Unit (GELU) activation, and layernormalization (LN), and this combination is repeated three times for initial feature extraction (Guo *et al* 2022). Following the encoding process, the feature maps undergo a symmetric decoding process, resulting in HRI feature maps. The framework further enters the interaction head, which facilitates the generation of segmentation outputs for hemorrhage and brain regions along with interaction classification.

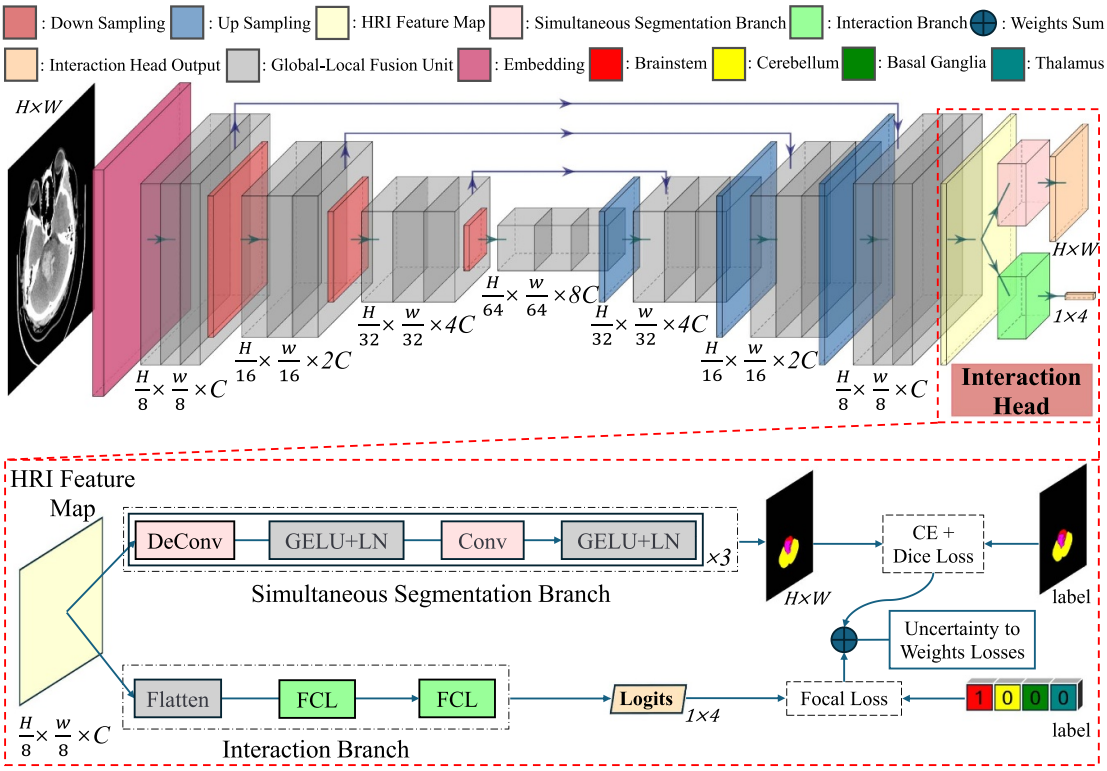

Figure 3. Overview of the proposed PHRI network, which features an interaction head designed to capture pairwise relationships, along with a GLFU to capture image-wide contextual information. The interaction head consists of a simultaneous segmentation branch and an interaction branch to segment hemorrhage and brain regions and classify the hemorrhage originating brain region, respectively.

2.1.1. Hemorrhage-brain regions interaction head

The hemorrhage-brain regions interaction head is designed to capture the relationships between hemorrhage and brain regions, inspired by the interaction detection head commonly used to identify pairwise interactions in HOI models (Tamura *et al* 2021, Kim *et al* 2022). A detailed illustration of this interaction head is provided in figure 3.

During the forward propagation phase, CT images undergo feature extraction via the encoder-decoder setup, culminating in the generation of a detailed HRI feature map while entering the interaction head. The detailed HRI feature map delineates the intricate hemorrhage-brain region relationships and is subsequently divided into two pathways: the simultaneous segmentation branch and the interaction branch, which together constitute the interaction head. The interaction branch is inspired by the use of the feedforward network to transform feature representations into a predictive interaction vector (Liu *et al* 2021, Tamura *et al* 2021, Kim *et al* 2022). In this branch, the HRI feature map is flattened and processed through two fully connected layers (FCLs), with the resulting vector serving as the final output for interaction classification. Meanwhile, the simultaneous segmentation branch employs a combination of deconvolution (DeConv), LN, GELU activation, and convolutional layers, with this combination repeated three times. This sequence reverses the embedding process and restores the feature map to its original dimensions, producing segmentation outputs for both hemorrhagic and critical brain regions, inspired by the expanding layer design in Guo *et al* (2022).

During the backpropagation, the interaction head is introduced to ensure that the HRI feature map serves as a conduit, facilitating effective information transfer between the simultaneous segmentation and interaction branches. Initially, the segmentation and interaction branches compute their losses. After applying uncertainty weighting, the features from both branches are integrated back into the HRI feature map. By encoding pairwise interactions as a learnable vector, where each component represents the hemorrhage in the corresponding brain region, the model directly captures the hemorrhage-region relationships within the HRI feature map. This allows the network to focus on relevant hemorrhage-brain region pairs, thereby improving feature extraction in both the segmentation and interaction branches. This pairwise interaction strategy also generalizes to cases with hemorrhages in multiple brain regions.

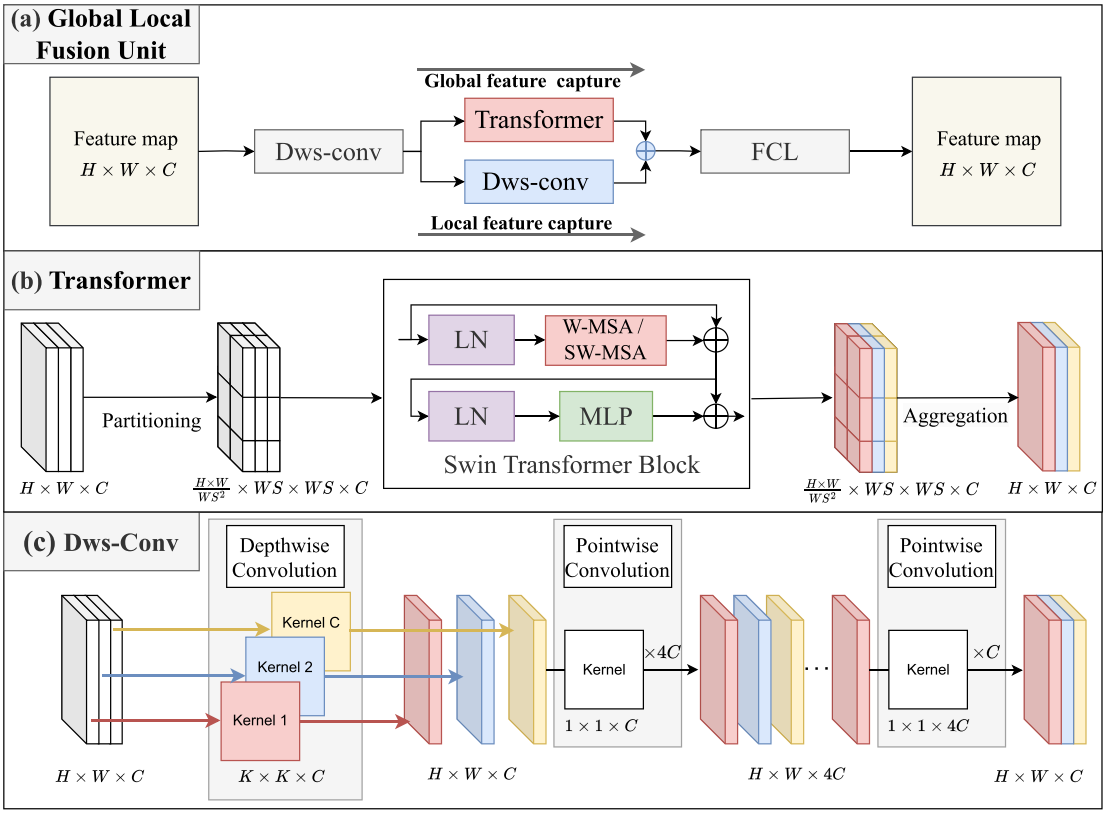

Figure 4. Detailed illustration of GLFU, highlighting the collaborative function of Depthwise Separable Convolution (Dws-Conv) and Transformer branches in enhancing image-wide contextual information. Sub-figure (a) depicts the overall GLFU architecture, while sub-figures (b) and (c) display the workflows of the Transformer and Dws-Conv branches, respectively.

2.1.2. GLFU

To provide the interaction head with comprehensive information, we propose the GLFU, which combines convolution and self-attention mechanisms. GLFU is a parallel branch unit that effectively integrates global and local information, offering two main advantages. First, it enables efficient fusion of global and local information, provided with contextual information. Second, it can seamlessly replace convolutional blocks in backbone architectures without disrupting their overall structure. As illustrated in figure 4(a), GLFU features two distinct parallel branches: Transformer and Depthwise Separable Convolution (Dws-Conv) (Chollet 2017). Initially, the input undergoes a Dws-Conv, and its outcomes are then processed using the parallel branches. The final process involves fusing the parallel branch outputs through an FCL.

2.1.2.1. Transformer branch

The Transformer branch utilizes the (Shift) Window Multi-head self-attention ((S)W-MSA) mechanism (Liu *et al* 2021) to efficiently extract and refine global information features, thereby enhancing the model's understanding of spatial relationships. There are two specially designed components in the Transformer branch. First, the Transformer branch conducts a systematic sequence of patch partitioning, (S)W-MSA, and patch aggregation, as illustrated in figure 4(b). These processes enable consistent feature extraction without altering the input and output dimensions of the feature map, making the Transformer branch compatible for integration with the GLFU. Second, the shift-window strategy was implemented to merge the cross-window information. This approach builds upon the initial partitioning window, shifting the sub-windows diagonally by a predetermined pixel distance to generate overlap. Within the pyramid hierarchy of a PHRI, each scale comprises three GLFUs, with the shift-window operation exclusively applied to the second GLFU.

The procedure for the Transformer branch is as follows. Initially, the Patch Partitioning phase divides the input feature map, denoted by $H \times W \times C$, into sub-windows with pre-defined dimensions $\frac{H \times W}{\mathrm{WS}^2} \times \mathrm{WS} \times \mathrm{WS} \times C$, where WS represents the sub-window size. Subsequently, the process enters the Swin Transformer Block (Liu *et al* 2021), wherein query, key, and value vectors are produced within each sub-window via linear transformations. MSA is employed to bolster global coherence and enrich the feature representation. Following MSA, a two-layer multilayer perceptron (MLP) with GELU activation further processes the output. An LN layer is applied before each MSA module and each MLP, and a residual

connection is applied after each module. Finally, the Patch Aggregation stage merges the processed sub-feature maps back to their original dimensions, $H \times W \times C$, ensuring the comprehensive preservation of refined features for subsequent processing.

2.1.2.2. Dws-Conv branch

The Dws-Conv branch is specifically designed to extract features from local information with high efficiency, as illustrated in figure 4(c). Each channel of the input feature map represented as $H \times W \times C$, is processed independently through depthwise convolution, using a separate convolutional kernel of size $K \times K$ for each of the C channels, with padding applied to preserve the output dimensions. This operation emphasizes the spatial features within the channels without inter-channel mixing. Subsequently, the first pointwise convolution (Pwconv) expands the feature dimension to 4 C, enabling cross-channel integration of features. Finally, a second Pwconv refines the feature map, reducing the dimensionality back to C. Through the design, the Dws-Conv branch ensures the extraction of local-rich features.

2.1.3. Training loss optimization

To train the proposed PHRI network more effectively, we utilized an uncertainty-weighted loss method for the simultaneous optimization. In this study, the segmentation task was optimized using a combination of Dice loss and cross-entropy (CE) loss, and the classification task was optimized with Focal loss. Ultimately, by applying the uncertainty weighting method to the loss functions, synchronized optimization was achieved.

2.1.3.1. Focal loss in interaction classification

In the realm of interaction classification, where class imbalance poses a significant challenge, Focal loss (Lin *et al* 2017) emerges as a pivotal tool. By integrating Focal loss, the model intensifies its focus on training instances associated with hemorrhage, thereby amplifying the impact of the harder-to-classify examples.

2.1.3.2. Dice and CE loss in segmentation

In our segmentation branch, our objective is to efficiently and synergistically segment hemorrhages and brain regions. To achieve this, we adopt a combined Dice+CE loss strategy, which integrates the class imbalance mitigation offered by Dice loss with the pixel-level classification precision of CE loss. Ma *et al* (2021) validates the robustness of the composite loss function. By leveraging the advantages of both losses, we can effectively address the issue of varying levels of label imbalance in the segmentation of brain regions and hemorrhages.

2.1.3.3. Uncertainty to weight losses

To optimize the weights of the segmentation and classification losses, we employ the uncertainty-weighted loss method proposed by Kendall *et al* (2018). This method derives a multi-task loss function based on maximising the Gaussian likelihood with homoscedastic uncertainty.

For each task, the method defines the likelihood as a Gaussian with the mean given by the model's output. Based on this assumption, in maximum likelihood inference, the method maximizes the log-likelihood, can be written as:

$$\log p\left(y \mid f^{W}(x)\right) \propto -\frac{1}{2\sigma^{2}} \| y - f^{W}(x) \|^{2} - \log \sigma. \tag{1}$$

Here, σ represents the model's observation noise parameter, where $f^{W}(x)$ is the output of model with weights W applied to the input x, and the model's output is denoted by y. Then, maximize this log-likelihood with respect to the model parameters W and the observation noise parameter σ. This is equivalent to minimizing the negative log-likelihood, which leads to the following minimization objective for our multi-output model: $\mathcal{L}(W, \sigma_{\text{seg}}, \sigma_{\text{cls}})$, representing our loss function.

$$\mathcal{L}\left(W, \sigma_{\text{seg}}, \sigma_{\text{cls}}\right) = -\log p\left(y_{\text{seg}}, y_{\text{cls}} \mid f^{W}(x)\right) = \frac{1}{2\sigma_{\text{seg}}^{2}} \mathcal{L}_{\text{seg}}(W) + \frac{1}{2\sigma_{\text{cls}}^{2}} \mathcal{L}_{\text{cls}}(W) + \log \sigma_{\text{seg}} \sigma_{\text{cls}}. \tag{2}$$

Finally, the method minimises the negative log-likelihood objective with respect to σ_{seg} and σ_{cls} as learning the relative weight of the losses $\mathcal{L}_{\text{seg}}(W)$ and $\mathcal{L}_{\text{cls}}(W)$ adaptively, based on the data.

2.1.4. Hemorrhage volume detection

2.1.4.1. Clinical adoption method

In clinical practice, the hemorrhage volume, which is crucial for surgical decision-making, is frequently estimated using the Coniglobus Formula. The formula, detailed in Hakimi and Garg (2016),

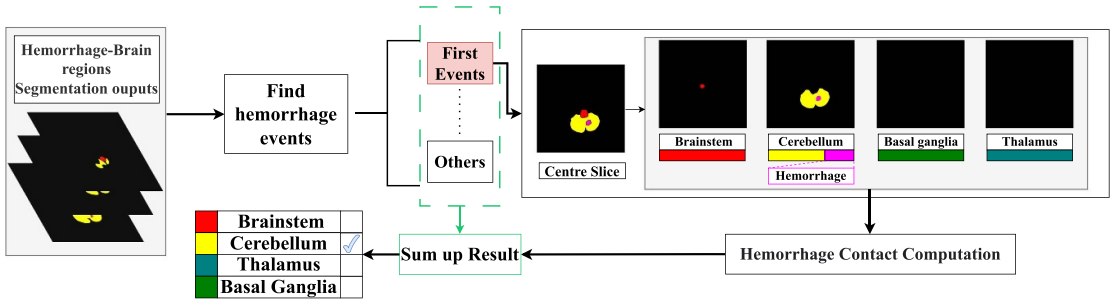

Figure 5. Schematic illustration of the clinical experience-based classification method.

Hillal *et al* (2022), is as follows:

$$\text{Hemorrhage Volume} = \frac{\text{Length} \times \text{Width} \times \text{Height}}{2}. \tag{3}$$

The Coniglobus Formula requires identifying the maximum cross-sectional area of the hemorrhage by measuring its greatest length and width, followed by determining the height by assessing the highest point perpendicular to this cross-sectional plane. However, this method has several limitations. Manual calculations by physicians can lead to variability, and the oversimplification may result in inaccurate volume estimations of irregularly shaped hemorrhages.

2.1.4.2. Voxel-based hemorrhage volume detection

In addition to the widely used Coniglobus formula, manual methods have been employed for volume estimation (Hillal *et al* 2022). These methods involve segmenting the hemorrhage, measuring the hematoma area, and multiplying it by the slice thickness. However, manual processes, particularly hand segmentation, are time-consuming. To address this issue, automatic approaches have been developed to expedite results by automating the segmentation process (Peng *et al* 2022). Our implementation adopts this approach while utilizing our PHRI segmentation results. Notably, the accuracy of the method is highly dependent on the quality of the segmentation results. Specifically, we first stack the 2D segmentation output slices along the z-axis to form a 3D hemorrhage volume, then calculate the number of voxels within the hemorrhage region, converting the voxel count into a volume measurement using voxel size information, as the equation as follows:

$$V_{\text{Hemorrhage}} = V_{\text{voxel}} \times N \tag{4}$$

$$V_{\text{voxel}} = s_x \times s_y \times t \tag{5}$$

where $V_{\text{Hemorrhage}}$ represents the total hemorrhage volume, V_{voxel} denotes the volume of each voxel, calculated as the product of s_x and s_y, which are the pixel spacing in the x- and y-directions, respectively, and t, the slice thickness in the z-direction, N represents the total number of voxels within the hemorrhage region, determined through image segmentation.

2.2. Clinical experience-based classification method

To provide a comparison with PHRI, we developed a clinical experience-based classification method to process the segmentation outcomes, as shown in figure 5. The developed method classifies the segmentation results into different IPH subtypes by computing the contact between hemorrhage and brain regions.

Following the segmentation of hemorrhages, the physician assessed the hemorrhage in alignment with the established clinical principles and professional judgment. Given the qualitative nature of a physician's insight, our analysis of the hemorrhage location was exclusively grounded in clinical principles as advised by our collaborating physicians. First, hemorrhage presenting as a homogeneous mass with continuity is typically classified as a singular hemorrhagic event. Depending on the patient, it is possible for there to be multiple homogeneous masses. Second, the classification of specific subtypes of hemorrhagic events is contingent upon analyzing the center of the hemorrhagic mass and its spatial relationship with adjacent brain regions.

Consequently, the initial step involves delineating the hemorrhagic events using connectivity analysis. Secondly, each hemorrhagic event is analyzed by identifying the central slice, which is the 2D slice with the

Table 1. Experiment setup of hemorrhagic stroke assessment.

Configuration	Parameters
GPU	GeForce RTX 4090 24GB
Deep learning framework	PyTorch 1.7
Learning rate	0.00 013
Batch size	8
Segmentation loss function	CE+Dice loss
Classification loss function	Focal loss Lin *et al* (2017)
Loss optimization strategy	Uncertainty-weighted loss Kendall *et al* (2018)
Optimizer	Adam

largest volume of hemorrhage. Subsequently, the degree of contact in the central slice is quantified for each event. Finally, all results of the hemorrhage events were summarized and considered as the classification outcome. To quantify the degree of contact, we employed a computational approach to calculate boundary contact

$$\text{Boundary contact rate} = \frac{\text{Contact boundary length}\,(\text{Hemorrhage}, \text{Critical brain regions})}{\text{Perimeter}\,(\text{Hemorrhage})}. \tag{6}$$

This formula calculates the ratio of the contact boundary length between the hemorrhage and critical brain regions to the total perimeter of the hemorrhage. The method uses contact boundary length(Hemorrhage, Critical brain regions) to measure the shared boundary length between the hemorrhage and the specified brain regions. Perimeter(Hemorrhage) is used to measure the total perimeter of the hemorrhage.

3. Experiments and results

3.1. Dataset and preprocessing

With institutional review board approval, an in-house hemorrhagic stroke CT scan dataset was collected, including 2764 CT slices from 99 patients. Each patient's scans consist of 20 to 35 axial slices, each with a thickness of 5 mm and pixel spacing ranging from 0.42 to 0.49 mm. Each slice has a resolution of 512 × 512 pixels.

An experienced radiologist meticulously drew masks for both the hemorrhagic areas and four key brain regions: the cerebellum, brain stem, basal ganglia, and thalamus. The hand-segmented masks served as reference standards in this study. Furthermore, CT imaging reports for all patients were collected, and the IPH classification labels were extracted from these reports. During the construction of the classification dataset, slices containing hemorrhage for each patient were labeled according to their CT imaging reports, while non-hemorrhagic slices were designated as negative samples. Finally, the classification dataset includes 157 cerebellum samples, 168 brainstem samples, 322 basal ganglia samples, and 135 thalamus samples, reflecting the distribution of critical brain regions affected by hemorrhage.

To validate the experiment's reliability, we performed five-fold cross-validation in both the comparison study and ablation study. The dataset was randomly partitioned into five folds in a patient-based manner. In each iteration, four folds were utilized for training and validation, and the remaining one was utilized for testing. The process was repeated five times until each of the five folds had been used as a testing set. Five-fold cross-validation verifies the credibility of the results. In data preprocessing, we normalized the data and applied common augmentation techniques, including random flips, rotations, Gamma transformations, and cropping, to mitigate potential overfitting and enhance model robustness.

3.2. Experimental environment and parameters

The proposed PHRI was achieved based on Python 3.7 and PyTorch 1.7. Our training environment was powered by an NVIDIA GeForce RTX 4090 equipped with 24 GB of VRAM. The initial learning rate was meticulously set to 0.00 013, with the Adam optimizer being instrumental in enhancing the model's performance. We stopped the training if the validation loss did not decrease in five epochs, and the network resulting in the lowest validation loss was selected and deployed on the test set. For segmentation tasks, a blend of CE and Dice loss functions was applied, while Focal loss (Lin *et al* 2017) was employed for classification objectives. An uncertainty-weighted loss (Kendall *et al* 2018) was selected as the loss optimization strategy. Details of the overall training configuration are delineated in table 1.

Table 2. Dice comparison across different models with mean values and standard deviations. Bold values highlight the best performance achieved for each brain region or hemorrhage category.

	Hemorrhage	Cerebellum	Brainstem
U-Net	0.8422 ± 0.3030	0.8710 ± 0.2666	0.8993 ± 0.2208
Segformer	**0.8819 ± 0.2502**	0.8933 ± 0.2225	0.9101 ± 0.1824
AttFocusNet	0.8750 ± 0.2627	0.8889 ± 0.2413	0.8996 ± 0.2147
OURs	0.8801 ± 0.2271	**0.9014 ± 0.1874**	**0.9218 ± 0.1481**
	Basal Ganglia	**Thalamus**	**Average**
U-Net	0.8415 ± 0.3048	0.8639 ± 0.3021	0.8636 ± 0.1666
Segformer	0.8881 ± 0.2407	0.9232 ± 0.2137	0.8991 ± 0.1298
AttFocusNet	0.8692 ± 0.2707	0.8943 ± 0.2609	0.8854 ± 0.1472
OURs	**0.8958 ± 0.2153**	**0.9330 ± 0.1784**	**0.9064 ± 0.1079**

Table 3. HD 95 comparison across different models with mean values and standard deviations. Bold values highlight the best performance achieved for each brain region or hemorrhage category.

	Hemorrhage	Cerebellum	Brainstem
U-Net	6.2139 ± 18.9362	6.9198 ± 14.0796	3.8990 ± 9.1804
Segformer	5.6515 ± 15.4741	6.8663 ± 13.1135	4.0836 ± 8.7792
AttFocusNet	5.7469 ± 17.3230	6.3560 ± 13.5147	3.5702 ± 7.4091
OURs	**4.5322 ± 12.2453**	**5.3918 ± 7.0335**	**3.0581 ± 3.6979**
	Basal Ganglia	**Thalamus**	**Average**
U-Net	5.7488 ± 14.7121	3.1642 ± 10.4990	5.1899 ± 7.3361
Segformer	5.8461 ± 14.8944	2.7643 ± 9.1743	5.0424 ± 6.6465
AttFocusNet	6.2323 ± 16.0610	3.2530 ± 10.6473	5.0317 ± 7.1491
OURs	**4.6495 ± 10.3236**	**2.5037 ± 6.5985**	**4.0271 ± 4.2409**

3.3. Results and evaluations

In the Experiment Result section, we will first compare our interaction classification as well as hemorrhage and brain region segmentation results with the state-of-the-art and use a T-TEST to provide persuasive evidence. To verify the capability of capturing interactions, experiments on Gard-CAM (Selvaraju *et al* 2019) were carried out. Secondly, the ablation study proves that the designs including GLFU and interaction head are effective. Finally, we compared the Coniglobus formula with our approach for computing hemorrhage volume.

3.3.1. Comparison with the competing methods

To validate the superiority of our proposed method, we evaluated the performance of different neural networks in segmentation, classification, and interaction visualization. We selected three competing segmentation models, including U-Net (Ronneberger *et al* 2015), AttFocusNet (Peng *et al* 2022), and Segformer (Xie *et al* 2021). U-Net is an encoder-decoder neural network architecture commonly used in the medical field. AttFocusNet is the newest version of U-Net that has been improved specifically for brain hemorrhage tasks. Segformer is a Transformer architecture designed for segmentation tasks. The following experiments include a comparison of segmentation and classification metrics, image visualization, and Grad-CAM.

3.3.1.1. Hemorrhage and brain-regions segmentation results

For the comparison of segmentation results, we chose the Dice coefficient, 95% Hausdorff Distance (HD 95), and Mean Intersection over Union (MIoU) as evaluation metrics, which are crucial in assessing the quality of segmentation. Tables 2–4 summarize the test results of different methods obtained from 5-fold cross-validation, presented as mean values with standard deviations. Based on these results, it is evident that the proposed method outperformed all competing methods in the average of all segmentation metrics.

A two-tailed paired T-TEST was conducted to examine the differences in pairwise performance metrics between our method (OURs) and other methods (U-Net, AttFocusNet, Segformer). As shown in table 5, the improvement in the average values of all segmentation performance metrics by our proposed method was statistically significant compared to the competing methods ($p < 0.05$).

Table 4. MIoU comparison across different models with mean values and standard deviations. Bold values highlight the best performance achieved for each brain region or hemorrhage category.

	Hemorrhage	Cerebellum	Brainstem
U-Net	0.8082 ± 0.3146	0.8375 ± 0.2842	0.8642 ± 0.2415
Segformer	0.8480 ± 0.2708	0.8567 ± 0.2522	0.8696 ± 0.2139
AttFocusNet	0.8420 ± 0.2796	0.8556 ± 0.2624	0.8627 ± 0.2379
OURs	**0.8623 ± 0.2460**	**0.8805 ± 0.2129**	**0.8985 ± 0.1759**
	Basal Ganglia	**Thalamus**	**Average**
U-Net	0.8106 ± 0.3251	0.8438 ± 0.3170	0.8329 ± 0.1829
Segformer	0.8569 ± 0.2739	**0.9036 ± 0.2387**	0.8670 ± 0.1495
AttFocusNet	0.8386 ± 0.2967	0.8742 ± 0.2809	0.8546 ± 0.1655
OURs	**0.8777 ± 0.2433**	0.8998 ± 0.2026	**0.8838± 0.1255**

Table 5. *P*-values for statistical significance tests across different average segmentation metrics.

Metric	OURs vs U-Net	OURs vs AttFocusNet	OURs vs Segformer
Dice	$P < 0.001$	$P < 0.001$	$P = 0.0162$
HD 95	$P < 0.001$	$P < 0.001$	$P < 0.001$
MIoU	$P < 0.001$	$P < 0.001$	$P = 0.0089$

Table 6. Comparative results across various models on different classification metrics. Bold values highlight the best classification performances.

	Hamming Loss	Overall Precision	Overall Recall	Overall F1-Score
U-Net	0.2176	0.6353	0.7714	0.6968
Segformer	0.1759	0.7463	0.7143	0.7299
AttFocusNet	0.2130	0.6623	0.7286	0.6939
OURs	**0.1157**	**0.7711**	**0.9143**	**0.8366**

3.3.1.2. IPH subtypes classification results

The IPH subtypes classification is the primary test task in this study, which is directly related to the quality of the relationships captured. To compare our classification results, we have chosen hamming loss, overall precision, overall recall, and overall F1-Score as classification metrics. These metrics are crucial for evaluating the multi-label classification tasks. Hemorrhages are typically ellipsoid in shape (Hillal *et al* 2022) and expand gradually from their origin (Qureshi *et al* 2001). Consequently, our framework uses the slice with the largest hemorrhage volume during testing to represent the central region and probable origin of the hemorrhage, serving as the basis for classification. For the three competing models, which did not directly output classification results, we applied the proposed clinical experience-based post-segmentation classification method to their outputs to obtain comparable classification results. Table 6 summarizes the classification test results of different methods obtained from five-fold cross-validations. The proposed method outperformed other competing methods in all classification metrics, with bold values highlighting the effectiveness of the proposed hemorrhage-brain regions interaction head.

3.3.1.3. Visual performance analysis

Figure 6 illustrates the segmentation results of different models in delineating hemorrhagic brain regions. Both scenarios, including those involving only brain regions and more complex cases with multiple brain regions and hemorrhages, are visualized. Our proposed method outperforms other models, particularly in complex cases where multiple brain regions and hemorrhage coexist.

3.3.1.4. Comparisons on Gradient-weighted Class Activation Mapping (Grad-CAM)

To further validate the relationship extraction capability of our method, we visualized and compared the Grad-CAM (Selvaraju *et al* 2019) of the aforementioned methods, as detailed in figure 7. We configured the target layers to the HRI feature map within the interaction head to assess interaction capture, while for the competing networks, the target layers were set to the corresponding feature layers. The target class was uniformly designated as hemorrhage. In the figure, the classification gold standard for row 1 is brain stem hemorrhage, row 2 is cerebellum hemorrhage, row 3 is basal ganglia hemorrhage and row 4 is concurrent hemorrhage in the basal ganglia and thalamus.

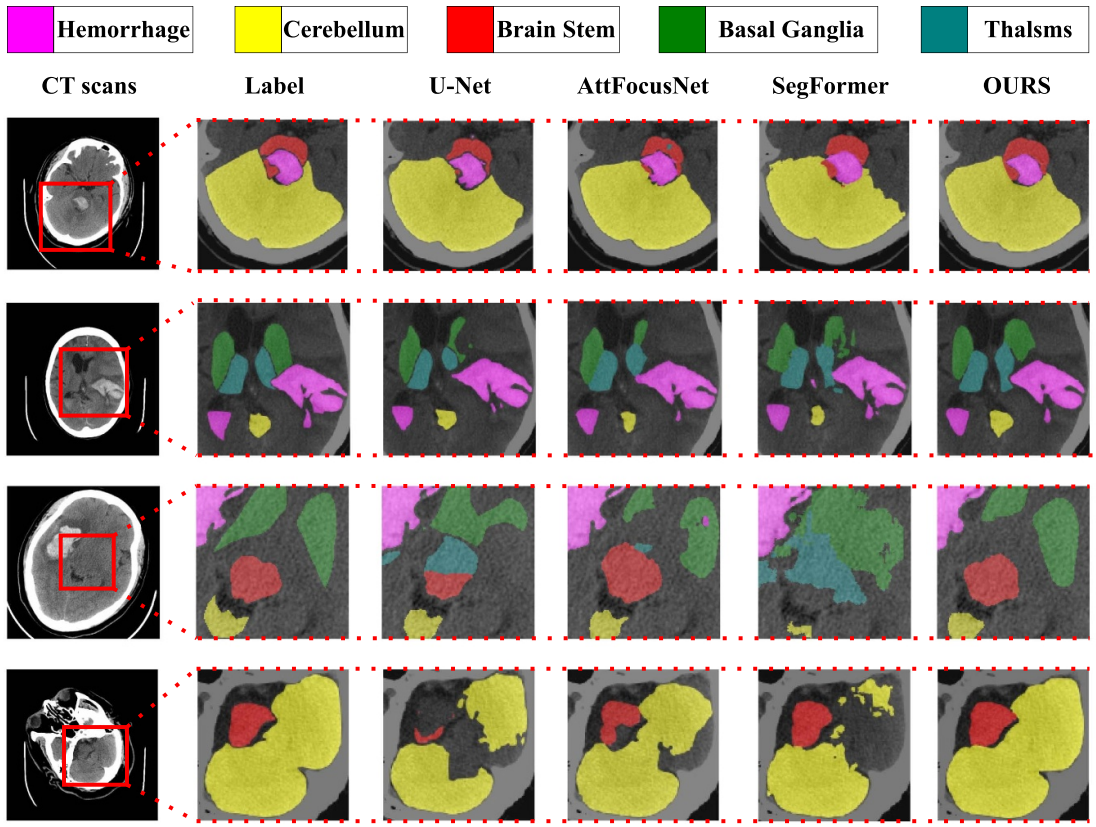

Figure 6. Visual comparison of segmentation outputs between our model and competing models.

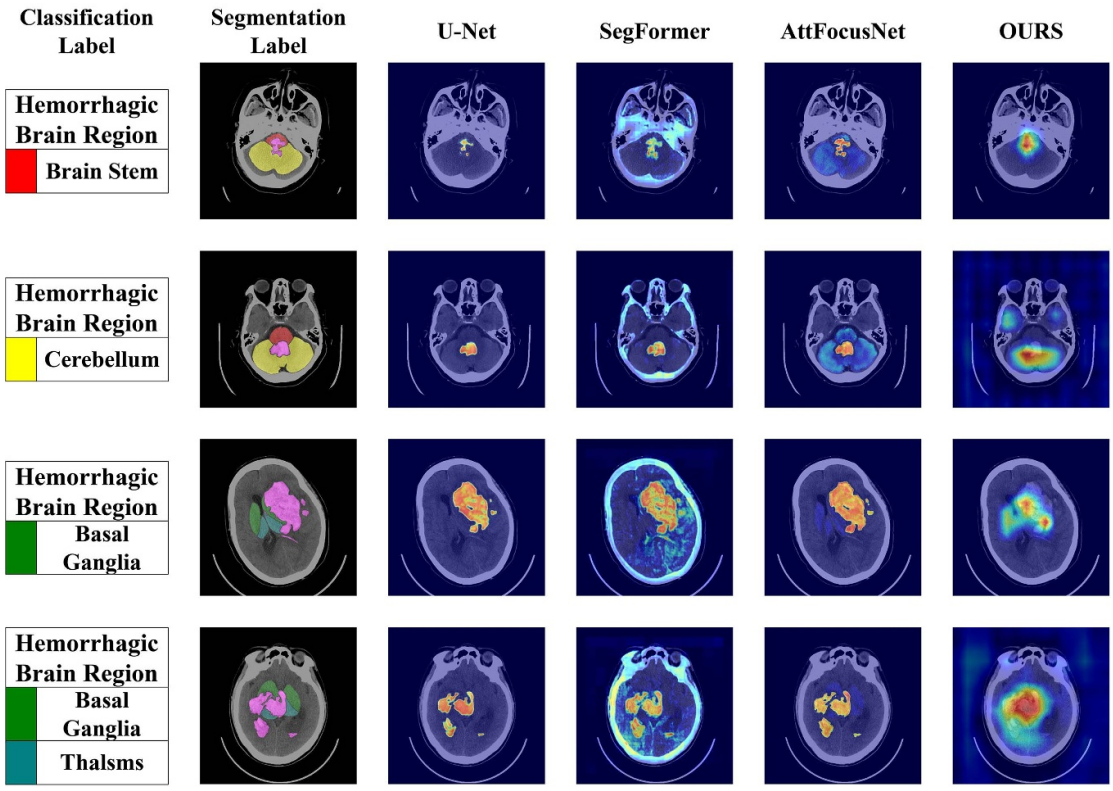

Figure 7. Examples of visual comparisons using Grad-CAM in the study highlight PHRI's ability to capture interactions between hemorrhages and critical brain regions, closely aligning with the labels. The hemorrhage label is represented in pink.

Table 7. Segmentation performance of model variants, illustrating incremental improvements from the baseline U-Net to more advanced configurations (+IDW, +ITR, +SSG, +MSG and +MSG+IH) across different metrics. Bold values indicate the best performance achieved in each metric.

	Dice(AVG)	HD 95(AVG)	MIoU(AVG)
Baseline(U-Net)	0.8636 ± 0.1666	5.1892 ± 7.3361	0.8328 ± 0.1829
+IDW	0.8867 ± 0.1301	4.4003 ± 5.9619	0.8566 ± 0.1474
+ITR	0.8965 ± 0.1295	4.4617 ± 5.9809	0.8676 ± 0.1475
+SSG	0.8942 ± 0.1303	4.0950 ± 6.0496	0.8638 ± 0.1483
+MSG	0.8975 ± 0.1282	4.2528 ±5.7763	0.8661 ± 0.1464
+MSG+IH	**0.9064 ± 0.1079**	**4.0271 ± 4.2409**	**0.8838 ± 0.1255**

Table 8. Classification performance of model variants, illustrating incremental improvements from the baseline U-Net to more advanced configurations (+IDW, +ITR, +SSG, +MSG and +MSG+IH) across different metrics. Bold values indicate the best performance achieved in each metric.

	Hamming Loss	Overall Precision	Overall Recall	Overall F1-Score
Baseline(U-Net)	0.2176	0.6353	0.7714	0.6968
+IDW	0.1864	0.6666	0.8011	0.7277
+ITR	0.1806	0.7222	0.8324	0.7734
+SSG	0.1528	0.7317	0.8571	0.7895
+MSG	0.1435	0.7468	0.8429	0.7919
+MSG+IH	**0.1157**	**0.7711**	**0.9143**	**0.8366**

According to Grad-CAM, we found that U-Net's attention is focused locally on the input, while Segformer can capture global information but lacks focus on relevant brain regions. AttFocusNet can detect the hemorrhage and all brain regions but lacks concentrated attention on the IPH-related brain regions. Our proposed model uniquely associates hemorrhage with the pertinent brain regions. For example, in rows 1 and 2, where the hemorrhage is in contact with both the cerebellum and brain stem, our model can distinguish different IPH types by focusing solely on the interaction-related critical brain region and hemorrhage.

3.3.2. Ablation study

We conducted an ablation study to validate the effectiveness of the proposed modules, as presented in tables 7 and 8. Several model variants were evaluated:

(1) Baseline (U-Net): standard encoder–decoder U-Net architecture.
(2) +IDW (Isolated Depthwise Separable Convolution branch): replace all the convolution blocks at all scales with the proposed GLFUs, but only retain the depthwise separable convolution branch within each GLFU, removing the transformer branch.
(3) +ITR (Isolation Transformer branch): replace all the convolution blocks at all scales with the proposed GLFUs, but only retain the transformer branch within each GLFU, removing the depthwise separable convolution branch.
(4) +SSG (Single-Scale GLFU): replace all the convolution blocks in the bottleneck scale of the encoder-decoder U-Net with the proposed GLFUs.
(5) +MSG (Multi-Scale GLFU): replace all the convolution blocks in all scales with the proposed GLFUs.
(6) +MSG+IH (Interaction Head): Integrates interaction head into the MSG to capture relational features, enabling segmentation and interaction classification outputs.

For both segmentation and classification, we used the same evaluation metrics as those used in comparing with competing methods. Similar to the comparison study, our proposed method involves selecting the slice with the largest hemorrhage volume to represent each patient's classification result. Additionally, the clinical experience-based post-segmentation classification method was applied to the baseline, +IDW, +ITR +SSG, and +MSG models, as these models did not produce direct classification outputs, allowing us to derive their classification results.

The results of the ablation study indicate that the addition of an interaction head or a gradual increase in GLFU has a beneficial effect on the outcomes of the segmentation and classification processes. Initially, integrating the GLFUs into the bottleneck scale (+SSG) enhances both the segmentation and classification capabilities of the network. This approach aligns with the implementation of the current CNN-Transformer models proposed for hemorrhage lesion segmentation (Nijiati *et al* 2022, Piao *et al* 2023). Subsequently, modifying from the Single-Scale GLFU, experiments confirms that extending the GLFUs to all scales

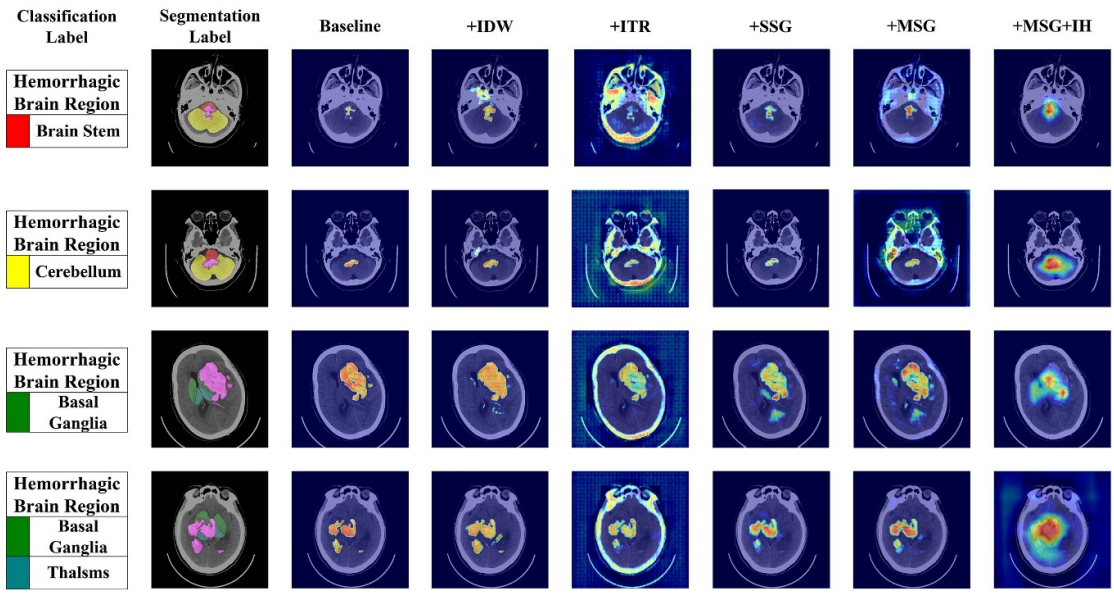

Figure 8. Examples of visual comparisons using Grad-CAM across the ablation study, showcase (+IH) enhanced ability to capture interactions between hemorrhages and critical brain regions, aligning closely with the labels. The hemorrhage label is represented in pink.

Table 9. Compared the consistency of the proposed method and the Coniglobus Formula with the gold standard in hemorrhage volume detection.

Method	Consistency
Coniglobus Formula	0.701
OURs	0.981

(+MSG) enables more efficient feature capture. Finally, incorporating the interaction head (+MSG+IH) allows the network to better capture pairwise hemorrhage-brain relationships, further improving classification and segmentation performance.

Furthermore, to evaluate the effectiveness of feature fusion derived from the standalone depthwise separable convolution and transformer branches, we conducted a comparative analysis between models incorporating only the depthwise separable convolution branch (+IDW), only the transformer branch (+ITR), and the GLFU maintaining both branches in parallel (+MSG). The results indicate that integrating both local and global feature fusion enhances the performances.

3.3.2.1. Comparisons on Grad-CAM

To further validate the effectiveness of the interaction head (+IH), we performed the Grad-CAM visualization analysis, with the same settings as in the comparison study, as detailed in figure 8. The results demonstrate how the heat map evolves as the proposed modules are incrementally integrated. Initially, we observed localized attention in the Baseline, and a similar pattern was maintained when applying depthwise separable convolution (+IDW). Introducing the GLFU at the bottleneck (+SSG) expands the attention field. Furthermore, when transformers are applied at all scales (+ITR and +MSG), the network captures global information but lacks precise focus on relevant brain regions. Finally, only with the application of the interaction head (+IH) does the network accurately direct its attention to both the hemorrhage and the corresponding brain regions.

3.3.3. Hemorrhage volume detection comparison

In this comparison, we evaluated the accuracy of the Voxel-Based Hemorrhage Volume Detection method applied to PHRI segmentation results against clinical practice using the Coniglobus Formula. The gold standard was established using manual volume estimation methods, based on radiologists meticulously drawing masks (Hillal *et al* 2022). To evaluate the results of hemorrhage volume detection, we applied the intraclass correlation coefficient (ICC) to assess the consistency and accuracy of our algorithm and the Coniglobus Formula with the gold standard, respectively. The results are shown in table 9 highlighting the superior performance of our method.

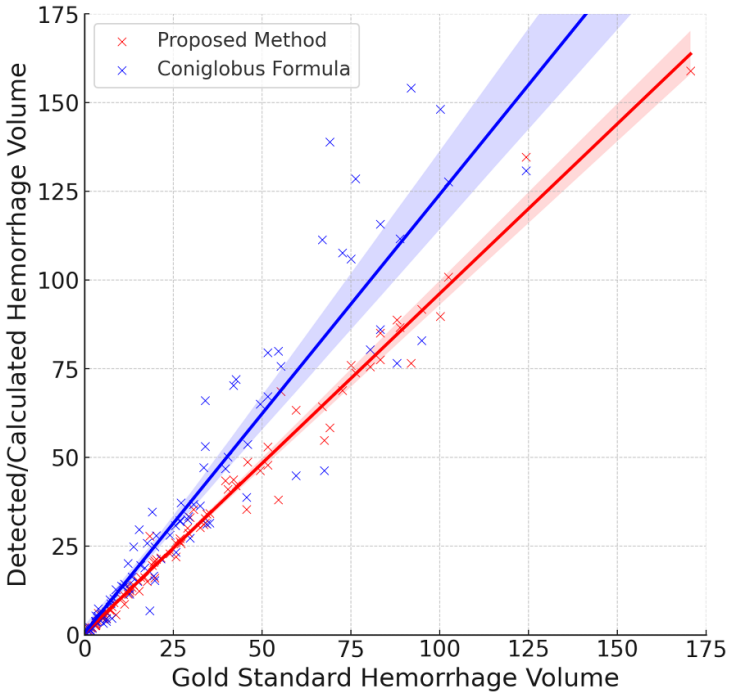

Figure 9. Consistency of hemorrhage volume detection: this plot compares the proposed method (red) and the Coniglobus Formula' (blue) against gold standard measurements.

We also demonstrated the effectiveness of our method with a scatterplot (figure 9) showing linear regression lines for actual and two method-estimated hemorrhage volumes. Confidence intervals on the regression lines highlight the precision and reliability of our method.

4. Discussion

This study explores a comprehensive hemorrhagic stroke assessment CAD system. Although earlier studies also have segmentation and classification methods related to hemorrhagic stroke, a method that portrays the relationships between hemorrhage and critical brain regions and meticulously diagnoses hemorrhage in brain regions is lacking. Therefore, we present a PHRI network, which can capture the relationships between hemorrhages and critical brain regions. Of greater significance, we apply the proposed network to conduct an in-depth assessment of hemorrhagic strokes, including hemorrhage segmentation, critical brain regions segmentation, IPH subtypes classification, and hemorrhage volume detection. The proposed CAD system has the potential to enhance personalized patient care, improve treatment outcomes, and increase the accuracy of prognostic assessments.

Our framework provides clinicians with essential, multifaceted hemorrhage information including a refined IPH classification method and a hemorrhage volume detection. Firstly, the current ICH classification method broadly localizes hemorrhages but often neglects the functional impacts on specific critical brain regions, limiting the customization and precision of treatment strategies. For instance, in the basal ganglia, stereotactic puncture is an effective minimally invasive procedure that reduces postoperative rebleeding risk (Zhu Suiqiang and Liying 2019), while blood pressure control is crucial for managing hemorrhage in this region (Al Fauzi 2020). Similarly, in the thalamus, stereotactic puncture is also a viable approach for treating hemorrhage (Lv and Wei 2021). In the thalamus, brain stems, and in cases of large hemorrhage, the resulting prolonged fever requires targeted treatment (Zhu Suiqiang and Liying 2019). In the brainstem, hemorrhage is primarily managed through conservative treatment, focusing on maintaining vital signs, controlling blood pressure and cerebral edema, and preventing complications (Chen 2021), while cerebellar hemorrhages that compress the brainstem necessitate immediate surgical intervention (Broderick 2007, Hostettler *et al* 2019, Zhu Suiqiang and Liying 2019). Thus, we propose a refined IPH classification method that accurately identifies hemorrhages in critical brain regions, facilitating more precise treatment planning. The classification results from the experiments validate the efficiency of the proposed method. Secondly, determining hemorrhage volume provides a crucial basis for doctors to assess the severity, guide treatment, and improve patient outcomes (LoPresti *et al* 2014). Compared to the Coniglobus formula, our proposed method for detecting hemorrhage volume demonstrates closer consistency with the gold standard.

Our network design effectively captures the interactions between hemorrhages and critical brain regions, offering two notable advantages. Firstly, emphasizing interactions between hemorrhages and critical brain regions significantly improves classification, resulting in reduced prediction of incorrect labels (hamming loss) and enhanced accurate identification of correct labels (overall precision, overall recall, and overall F1-score). Secondly, emphasizing interactions enhances segmentation capabilities, as evidenced by the improved segmentation performance observed in the ablation study with the addition of the interaction head. This enhancement is potentially attributed to the interactions' ability to effectively manage scenarios involving multiple brain regions and hemorrhages. The Grad-CAM visualizations in figures 7 and 8 demonstrate that the network with the interaction head can differentiate similar cases with multiple brain regions, such as brain stem and cerebellum involvement (rows 1 and 2) and basal ganglia and thalamic involvement (rows 3 and 4). Despite these similarities, the network effectively distinguishes between different conditions, focusing on the hemorrhage and the associated brain regions. As depicted in figure 6, the visual segmentation results involving multiple brain regions and hemorrhages, particularly in the first three rows, demonstrate that our model accurately and comprehensively distinguishes and segments cases involving multiple brain regions and coexisting hemorrhages.

Nevertheless, this research has its limitations. The training dataset necessitates a significant workload for labeling, including hemorrhage masks, brain region masks, and hemorrhage classification obtained from imaging reports, resulting in a limited dataset size. We will continue to expand our dataset to further enhance the performance of our CAD framework. However, establishing a gold standard for segmentation and classification suitable for CAD tasks constitutes a significant effort. To alleviate the burden on medical practitioners and to improve the robustness of our model, we intend to explore semi-supervised or unsupervised methodologies to augment the training dataset. Furthermore, given the critical need for timely and accurate diagnosis in hemorrhagic stroke cases (George 2017), the proposed framework focuses on CT, the preferred initial screening tool for stroke diagnosis in clinical practice. However, incorporating additional imaging modalities could provide valuable complementary information in specific conditions (Hakimi and Garg 2016). Thus, in future work, we plan to integrate multimodal imaging to enhance the understanding of ICH.

5. Conclusion

In conclusion, this study presents a comprehensive CAD system for the diagnosis of hemorrhagic stroke. We propose a PHRI network, which is capable of capturing the relationships between hemorrhages and critical brain regions. Importantly, we apply the proposed network to conduct an in-depth assessment of hemorrhagic strokes, including hemorrhage segmentation, critical brain regions segmentation, IPH subtypes classification, and hemorrhage volume detection. Experimental results showed the superior performances of the proposed CAD method, outperforming several state-of-the-art methods. Moreover, we conducted ablation studies to verify the effectiveness of each proposed module. The proposed CAD system has the potential to enhance personalized patient care, improve treatment outcomes, and increase the accuracy of prognostic assessments.

Data availability statement

All data that support the findings of this study are included within the article (and any supplementary information files).

Acknowledgment

This work is supported by the Guangdong Basic and Applied Basic Research Foundation under Grant 2023A1515011488, and supported by STU Scientific Research Foundation for Talents NTF21004.

ORCID iDs

Wei Liang https://orcid.org/0009-0007-5618-8961
Hongbin Guo https://orcid.org/0009-0005-4518-0740
Zhanyao Huang https://orcid.org/0009-0001-5958-3322
Shibin Liang https://orcid.org/0009-0006-4475-2943
Xiangyuan Ma https://orcid.org/0000-0002-8107-6861

References

Al Fauzi A *et al* 2020 Epidemiology of intra-cerebral hemorrhage in young adult patients *JUXTA* **11** 65–68

Arman S E, Saminur Rahman S, Irtisam N, Ahmed Deowan S, Ariful Islam Md, Sakib S and Hasan M 2023 Intracranial hemorrhage classification from ct scan using deep learning and bayesian optimization *IEEE Access* **11** 83446–60

Broderick J *et al* 2007 Guidelines for the management of spontaneous intracerebral hemorrhage in adults: 2007 update: A guideline from the american heart association/american stroke association stroke council, high blood pressure research council and the quality of care and outcomes in research interdisciplinary working group: The american academy of neurology affirms the value of this guideline as an educational tool for neurologists *Stroke* **38** 2001–23

Chen D *et al* 2021 Primary brainstem hemorrhage: a review of prognostic factors and surgical management *Front. Neurol.* **12** 727962

Chilamkurthy S, Ghosh R, Tanamala S, Biviji M, Campeau N G, Kumar Venugopal V, Mahajan V, Rao P and Warier P 2018 Deep learning algorithms for detection of critical findings in head ct scans: a retrospective study *Lancet* **392** 2388–96

Cho H, Kim C, Kim J, Lee S, Ismayilzada E and Baek S 2023 Transformer-based unified recognition of two hands manipulating objects *Proc. IEEE/CVF Conf. on Computer Vision and Pattern Recognition* pp 4769–78

Chollet F 2017 Xception: Deep learning with depthwise separable convolutions *Proc. IEEE Conf. on Computer Vision and Pattern Recognition* pp 1251–8

Coorens N A, Groot Lipman K, Krishnam S P, Ozan Tan C, Alic L and Gupta R 2023 Intracerebral hemorrhage segmentation on noncontrast computed tomography using a masked loss function u-net approach *J. Comput. Assist. Tomogr.* **47** 93–101

Dhar R *et al* 2020 Deep learning for automated measurement of hemorrhage and perihematomal edema in supratentorial intracerebral hemorrhage *Stroke* **51** 648–51

ElZemity A, ElFdaly M, Abdelfattah S, Abdelwahab A, Ramadan M, Zakzouk S, Ameen A, Elkhishen R and Saeed Darweesh M 2023 A transformer-based deep learning architecture for accurate intracranial hemorrhage detection and classification *Int. Conf. on Innovation and Intelligence for Informatics, Computing and Technologies* pp 215–20

Feigin V L *et al* 2021 Global, regional and national burden of stroke and its risk factors, 1990–2019: a systematic analysis for the global burden of disease study 2019 *Lancet Neurol.* **20** 795–820

Fujita H 2020 Ai-based computer-aided diagnosis (AI-CAD): the latest review to read first *Radiol. Phys. Technol.* **13** 6–19

George M G 2017 Cdc grand rounds: public health strategies to prevent and treat strokes *Morbidity and Mortality Weekly Report* **66**

Guo J, Zhou H-Y, Wang L and Yu. Y 2022 Unet-2022: exploring dynamics in non-isomorphic architecture *Int. Conf. on Medical Imaging and Computer-Aided Diagnosis* (Springer) pp 465–76

Hakimi R and Garg A 2016 Imaging of hemorrhagic stroke *CONTINUUM: Lifelong Learn. Neurol.* **22** 1424–50

Hillal A, Ullberg T, Ramgren B and Wassélius J 2022 Computed tomography in acute intracerebral hemorrhage: neuroimaging predictors of hematoma expansion and outcome *Insights Imaging* **13** 180

Hostettler I C, Seiffge D J and Werring D J 2019 Intracerebral hemorrhage: an update on diagnosis and treatment *Exp. Rev. Neurother.* **19** 679–94

Ibrahim A H, Mohamad N, Mohd Yusof Rasid T A and Abdullah M S 2022 Cerebellar hemorrhage in a healthy young adult: a case report *J. Med. Case Rep.* **16** 380

Kaae Andersen K, Skyhøj Olsen T, Dehlendorff C and Peter Kammersgaard L 2009 Hemorrhagic and ischemic strokes compared: stroke severity, mortality and risk factors *Stroke* **40** 2068–72

Kendall A, Gal Y and Cipolla R 2018 Multi-task learning using uncertainty to weigh losses for scene geometry and semantics *Proc. IEEE Conf. on Computer Vision and Pattern Recognition* pp 7482–91

Kim B, Mun J, On K-W, Shin M, Lee J and Kim E-S 2022 Mstr: Multi-scale transformer for end-to-end human-object interaction detection *Proc. IEEE/CVF Conf. on Computer Vision and Pattern Recognition* pp 19578–87

Lin T-Y, Goyal P, Girshick R, Kaiming H and Dollár P 2017 Focal loss for dense object detection *Proc. IEEE Int. Conf. on Computer Vision* pp 2980–8

Liu Z, Lin Y, Cao Y, Hu H, Wei Y, Zhang Z, Lin S and Guo B 2021 Swin transformer: Hierarchical vision transformer using shifted windows *Proc. IEEE/CVF Int. Conf. on Computer Vision* pp 10012–22

LoPresti M A, Bruce S S, Camacho E, Kunchala S, Dubois B G, Bruce E, Appelboom G and Sander Connolly E 2014 Hematoma volume as the major determinant of outcomes after intracerebral hemorrhage *J. Neurol. Sci.* **345** 3–7

Lv Y and Wei W 2021 Clinical treatment progress of small amounts thalamus hemorrhage *Brain Hemorrhages* **2** 84–87

Ma J, Chen J, Ng M, Huang R, Li Y, Li C, Yang X and Martel A L 2021 Loss odyssey in medical image segmentation *Med. Image Anal.* **71** 102035

Macellari F, Paciaroni M, Agnelli G and Caso V 2014 Neuroimaging in intracerebral hemorrhage *Stroke* **45** 903–8

Manjurul Ahsan Md, Akter Luna S and Siddique Z 2022 Machine-learning-based disease diagnosis: a comprehensive review *Healthcare* **10** 541

McGurgan I J, Ziai W C, Werring D J, Al-Shahi Salman R and Parry-Jones A R 2021 Acute intracerebral haemorrhage: diagnosis and management *Pract. Neurol.* **21** 128–36

McLouth J, Elstrott S, Chaibi Y, Quenet S, Chang P D, Chow D S and Soun J E 2021 Validation of a deep learning tool in the detection of intracranial hemorrhage and large vessel occlusion *Front. Neurol.* **12** 656112

Nijiati M, Tuersun A, Zhang Y, Yuan Q, Gong P, Abulizi A, Tuoheti A, Abulaiti A and Zou X 2022 A symmetric prior knowledge based deep learning model for intracerebral hemorrhage lesion segmentation *Front. Physiol.* **13** 977427

Park J 2016 Movement disorders following cerebrovascular lesion in the basal ganglia circuit *J. Movement Disorders* **9** 71

Park J, Park J-W and Lee J-S 2023 Viplo: vision transformer based pose-conditioned self-loop graph for human-object interaction detection *Proc. IEEE/CVF Conf. on Computer Vision and Pattern Recognition* pp 17152–62

Peng Q, Chen X, Zhang C, Wenyan Li, Liu J, Shi T, Wu Y, Feng H, Nian Y and Rong H 2022 Deep learning-based computed tomography image segmentation and volume measurement of intracerebral hemorrhage *Front. Neurosci.* **16** 965680

Piao Z, Gu Y H, Jin H and Joon Yoo S 2023 Intracerebral hemorrhage ct scan image segmentation with hardnet based transformer *Sci. Rep.* **13** 7208

Qureshi A I, Tuhrim S, Broderick J P, Hunt Batjer H, Hondo H and Hanley D F 2001 Spontaneous intracerebral hemorrhage *New Engl. J. Med.* **344** 1450–60

Retuci Pinheiro G, Brusini L, Carmo D, Prôa R, Abreu T, Appenzeller S, Menegaz G and Rittner L 2023 Thalamus segmentation using deep learning with diffusion MRI data: an open benchmark *Appl. Sci.* **13** 5284

Ronneberger O, Fischer P and Brox T 2015 U-net: Convolutional networks for biomedical image segmentation *Medical Image Computing and Computer-Assisted Intervention* (Springer) pp 234–41

Selvaraju R R, Cogswell M, Das A, Vedantam R, Parikh D and Batra D 2019 Grad-cam: visual explanations from deep networks via gradient-based localization *Int. J. Comput. Vis.* **128** 336–59
Shu X, Chang F, Zhang X, Shao C and Yang X 2022 Ecau-net: Efficient channel attention u-net for fetal ultrasound cerebellum segmentation *Biomed. Signal Process. Control* **75** 103528
Su C, Chen H, Kwan A, Lin Y and Guo N 2007 Neuropsychological impairment after hemorrhagic stroke in basal ganglia *Arch. Clin. Neuropsychol.* **22** 465–74
Sugino T, Kin T, Saito N and Nakajima Y 2024 Improved segmentation of basal ganglia from mr images using convolutional neural network with crossover-typed skip connection *Int. J. Comput. Assist. Radiol. Surg.* **19** 433–42
Tamura M, Ohashi H and Yoshinaga T 2021 Qpic: query-based pairwise human-object interaction detection with image-wide contextual information *Proc. IEEE/CVF Conf. on Computer Vision and Pattern Recognition* pp 10410–9
Temel M, Polat B S A, Kayali N and Karadas O 2021 Cognitive profile of patients with thalamic hemorrhage according to lesion localization *Dementia Geriat. Cogn. Disorders Extra* **11** 129–33
Tu D, Sun W, Zhai G and Shen W 2023 Agglomerative transformer for human-object interaction detection *Proc. IEEE/CVF Int. Conf. on Computer Vision* pp 21614–24
Umapathy S, Murugappan M, Bharathi D and Thakur M 2023 Automated computer-aided detection and classification of intracranial hemorrhage using ensemble deep learning techniques *Diagnostics* **13** 2987
Wang X, Liu Z, Li J and Xiong G 2022 Vision transformer-based classification study of intracranial hemorrhage *Int. Conf. on Computer Vision, Image and Deep Learning & Int. Conf. on Computer Engineering and Applications* pp 1–8
World Stroke Organization 2022 Global stroke fact sheet 2022 *Int. J. Stroke* **17** 478
Xiao Y, Hou Y, Wang Z, Zhang Y, Xuanya Li, Kai H and Gao X 2024 Multi-scale perception and feature refinement network for multi-class segmentation of intracerebral hemorrhage in ct images *Biomed. Signal Process. Control* **88** 105614
Xie E, Wang W, Yu Z, Anandkumar A, Alvarez J M and Luo P 2021 Segformer: simple and efficient design for semantic segmentation with transformers *Advances in Neural Information Processing Systems* vol 34 pp 12077–90
Zhang F Z, Yuan Y, Campbell D, Zhong Z and Gould S 2023 Exploring predicate visual context in detecting of human-object interactions *Proc. IEEE/CVF Int. Conf. on Computer Vision* pp 10411–21
Zhang J, Liang W, Guo H, Zhang H, Xu Z and Ma X 2024 Dual-path u-transformer network for assessment of brain midline shift in hemorrhagic stroke *15th Int. Conf. on Graphics and Image Processing* vol 13089 (SPIE) pp 345–53
Zhu Suiqiang L M and Liying C 2019 Chinese guidelines for diagnosis and treatment of acute intracerebral hemorrhage 2019 *Chin. J. Neurol.* **52** 994–1005